Density profiles around $A + B \rightarrow C$ reaction-diffusion fronts in partially miscible systems: A general classification

V. Loodts,[1] P. M. J. Trevelyan,[2] L. Rongy,[1] and A. De Wit[1,*]

[1]*Université libre de Bruxelles (ULB), Faculté des Sciences, Nonlinear Physical Chemistry Unit, Campus de la Plaine - Boulevard du Triomphe CP231 1050 Bruxelles, Belgium*

[2]*Division of Mathematics and Statistics, University of South Wales, Pontypridd CF37 1DL, United Kingdom*

(Received 25 July 2016; published 28 October 2016)

Various spatial density profiles can develop in partially miscible stratifications when a phase A dissolves with a finite solubility into a host phase containing a dissolved reactant B. We investigate theoretically the impact of an $A + B \rightarrow C$ reaction on such density profiles in the host phase and classify them in a parameter space spanned by the ratios of relative contributions to density and diffusion coefficients of the chemical species. While the density profile is either monotonically increasing or decreasing in the nonreactive case, reactions combined with differential diffusivity can create eight different types of density profiles featuring up to two extrema in density, at the reaction front or below it. We use this framework to predict various possible hydrodynamic instability scenarios inducing buoyancy-driven convection around such reaction fronts when they propagate parallel to the gravity field.

DOI: 10.1103/PhysRevE.94.043115

I. INTRODUCTION

The study of partially miscible stratifications has recently gained interest due to its relevance for groundwater management [1,2], enhanced oil recovery [3–5], or carbon dioxide (CO_2) sequestration [5–14]. Such stratifications are typically composed of a reservoir phase A dissolving with a finite solubility into a host phase, containing chemicals that may react with A. The dissolution of A is limited by its solubility in the host phase, where most of the dynamics occurs [12–18]. Upon dissolution and reaction, various concentration profiles can develop and thereby affect the physical properties of the host phase.

In particular, dynamic changes in concentrations can induce spatiotemporal variations of the density of the solution, which in turn can generate hydrodynamic buoyancy-driven instabilities [19]. As an example, Rayleigh-Taylor convection can develop when locally a denser zone overlies a less dense one in the gravity field [20] or gravity currents can also arise from horizontal density gradients [21,22]. In the case of partially miscible interfaces, so-called dissolution-driven convection can also develop when the transfer of one phase into the other one locally changes the density of the host solution upon dissolution [23,24]. This is the case, for instance, during dissolution from above of less dense CO_2 or of an ester into aqueous solutions [12–18] or upon dissolution from below of methanol into cyclohexane [25].

We thus see that changes of density gradients by reaction-diffusion processes during dissolution in partially miscible systems can be the source of convective motions affecting mixing and the transfer from one phase to the other. Classifying the possible density profiles developing around $A + B \rightarrow C$ reaction-diffusion fronts in such partially miscible systems is therefore crucial to understanding the onset of possible buoyancy-driven instabilities. It also helps to predict the spatial zones in which convection could be localized in cases of nonmonotonic density profiles i.e., spatial profiles featuring local extrema [26–29].

Density profiles have already been classified in the case of a miscible interface between two solutions containing solutes A and B. In the nonreactive case, six different density profiles can develop depending on the relative contribution of A and B to density and the ratio of their diffusion coefficients [30]. In the reactive case where an $A + B \rightarrow C$ reaction takes place, six different profiles are also possible if all species diffuse at the same rate [31,32]. On the contrary, if differential diffusion is taken into account, the number of possible density profiles increases up to 62 in the miscible case [33].

For partially miscible stratifications, the possible density profiles have been classified in the case where all species diffuse at the same rate [15,16]: Without reaction, only two density profiles can build up, monotonically increasing or decreasing [16]. The number of possible density profiles increases up to four when a reaction $A + B \rightarrow C$ takes place in the host phase [15,16]. If the nonreactive profile can be buoyantly unstable, i.e., the density of the solution increases upon dissolution, a minimum of density is formed when C contributes less to density than B, which slows down the growth of buoyancy-driven fingering [15–17]. If C is sufficiently denser than B, the density profile remains monotonic and the reaction can accelerate the development of the instability [15,16]. Chemistry can even be at the origin of the instability by creating a maximum of density when the dissolving species decreases or does not modify density [16,34–38]. Similarly to what has been done in miscible stratifications [33], a classification of the possible density profiles is now needed for partially miscible systems in the more general case where species can diffuse at different rates.

In this context, we analyze here theoretically the reaction-diffusion (RD) density profiles building up in a partially miscible system when a species A dissolves into a host solution of B and an $A + B \rightarrow C$ reaction takes place in the host phase. We classify these profiles in a parameter space spanned by the diffusivity and solutal expansion coefficient ratios. To

*adewit@ulb.ac.be

 ©2016 American Physical Society

do so, we derive asymptotic concentration profiles from the classical RD equations. By reconstructing the density profiles in the host solution, we show that eight different types of RD density profiles can be observed, with zero, one, or two extrema at the reaction front or below. Each type of RD density profile will lead to a different scenario for the development of buoyancy-driven convection. The classification developed here can be used as a framework to unify previous results as well as predict potential dynamics in unexplored parameter zones.

This work is structured as follows. The model and the equations are presented in Sec. II. We compute the asymptotic concentration profiles in Sec. III and construct the related RD density profiles both above and below the reaction front in Sec. IV. Section V gives more details about the extrema of density below the reaction front. The global density profiles are described in Sec. VI and compared to their counterparts in miscible stratifications in Sec. VII. Finally, we summarize this study in Sec. VIII.

II. MODEL

Let us consider an isothermal partially miscible system in which a reservoir phase A is placed in contact with a host phase along a planar interface located at $z = 0$ with z pointing into the host phase (Fig. 1). Although this study is valid for any orientation of the z axis with regard to gravity, Fig. 1 illustrates the special case where the interface is at the top of the host phase, which is the case, for instance, in the convective dissolution of CO_2 into brine during CO_2 sequestration [6,7,12–14]. The host phase contains a dissolved reactant B in initial concentration B_0. Phase A dissolves in the course of time into the host phase and reacts with B according to the $A + B \to C$ scheme. This bimolecular reaction is considered to occur as an elementary step so that its rate is given by qAB, with q the kinetic constant and A and B the concentrations of species A and B, respectively.

In order to model the dynamics in the host phase, we make the following assumptions. At the interface, the concentration of A is equal to its solubility A_0 in the host phase (local chemical equilibrium). This value is not limited by the concentration of A in the reservoir phase and does not evolve over time. Moreover, we suppose that A_0 does not depend on the concentrations of B or C. This approximation is valid as long as the initial concentration B_0 of the solute B in solution is small enough [14]. No mass transfer takes place from the host phase to the reservoir phase A.

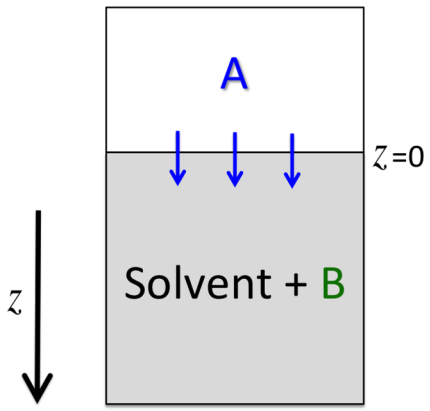

FIG. 1. Schematic of a two-layer partially miscible stratification, where the reservoir phase A dissolves with a finite solubility into the host phase (shaded) containing a dissolved reactant B.

The RD equations governing the evolution of the concentration profiles A, B, and C in the host phase are

$$\frac{\partial A}{\partial t} = D_A \frac{\partial^2 A}{\partial z^2} - qAB, \tag{1a}$$

$$\frac{\partial B}{\partial t} = D_B \frac{\partial^2 B}{\partial z^2} - qAB, \tag{1b}$$

$$\frac{\partial C}{\partial t} = D_C \frac{\partial^2 C}{\partial z^2} + qAB, \tag{1c}$$

where the molecular diffusion coefficients D_i are assumed constant for each species $i = A$, B, and C. To describe the convective dynamics in the host phase, Eqs. (1) can be coupled to an equation for the velocity of the fluid. We explicitly do not detail the flow equation here as we aim to classify the density profiles before the onset of convection, i.e., when there is still no fluid flow. In this limit, the profiles governed by reaction and diffusion processes depend on the z direction only. Our approach is thus generic, in other words, valid for any flow equation, e.g., Darcy's law in porous media and Hele-Shaw cells, and Stokes or Navier-Stokes equations in other cases [20]. The buoyancy term $\rho \boldsymbol{g}$ typically appears in such a flow equation, where $\boldsymbol{g}$ is the gravity field and ρ is the density of the solution depending on the concentrations. In a diluted solution, this dependence is assumed to be linear [9] as

$$\rho = \rho_0(1 + \alpha_A A + \alpha_B B + \alpha_C C), \tag{2}$$

where ρ_0 is the density of the solvent of the host phase and $\alpha_i = \frac{1}{\rho_0}\frac{\partial \rho}{\partial i}$ is the solutal expansion coefficient of species i.

To solve Eqs. (1), we use the initial conditions

$$A = A_0 \quad \text{for } z = 0, \quad A = 0 \quad \text{for } z > 0, \tag{3a}$$

$$B = B_0, \quad C = 0 \quad \forall z \tag{3b}$$

and the boundary conditions

$$A = A_0, \quad \frac{\partial B}{\partial z} = 0, \quad \frac{\partial C}{\partial z} = 0 \quad \text{for } z = 0, \tag{4a}$$

$$A \to 0, \quad B \to B_0, \quad C \to 0 \quad \text{for } z \to \infty. \tag{4b}$$

We nondimensionalize Eqs. (1) by introducing the dimensionless time $\tilde{t} = t/t_c$, space coordinate $\tilde{z} = z/l_c$, concentrations $[\tilde{A}, \tilde{B}, \tilde{C}] = [A, B, C]/A_0$, and density $\tilde{\rho} = (\rho - \rho_0)/\rho_c$, with $t_c = 1/(qA_0)$ and $l_c = \sqrt{D_A t_c}$, the characteristic RD time and length scales [15,16,31,32], respectively, and ρ_c a characteristic density whose expression depends on the flow equation. For example, if Darcy's law is used, $\rho_c = \mu D_A/(\kappa l_c g)$, with μ the viscosity of the solvent, κ the permeability of the porous medium, and g the norm of the gravity field.

Substituting these dimensionless variables into Eqs. (1) and (2) and dropping tildes for convenience leads to the

dimensionless equations

$$\frac{\partial A}{\partial t} = \frac{\partial^2 A}{\partial z^2} - AB, \tag{5a}$$

$$\frac{\partial B}{\partial t} = \delta_B \frac{\partial^2 B}{\partial z^2} - AB, \tag{5b}$$

$$\frac{\partial C}{\partial t} = \delta_C \frac{\partial^2 C}{\partial z^2} + AB, \tag{5c}$$

$$\rho = R_A A + R_B B + R_C C. \tag{5d}$$

Here $\delta_i = D_i/D_A$ is the ratio of diffusion coefficient of species i to that of the dissolving species A. The Rayleigh number $R_i = \alpha_i A_0 \rho_0/\rho_c$ of species i quantifies the relative contribution of i to density; R_i can be positive, zero, or negative, depending on whether species i increases ($\alpha_i > 0$), does not modify ($\alpha_i = 0$), or decreases ($\alpha_i < 0$) the density of the solution.

The initial conditions (3) are nondimensionalized as

$$A = 1 \quad \text{for } z = 0, \quad A = 0 \quad \text{for } z > 0, \tag{6a}$$

$$B = \beta, \quad C = 0 \quad \forall z, \tag{6b}$$

where $\beta = B_0/A_0$ is the ratio of the initial concentration of B and the solubility of A in the host phase. Similarly, boundary conditions (4) become

$$A = 1, \quad \frac{\partial B}{\partial z} = 0, \quad \frac{\partial C}{\partial z} = 0 \quad \text{for } z = 0, \tag{7a}$$

$$A \rightarrow 0, \quad B \rightarrow \beta, \quad C \rightarrow 0 \quad \text{for } z \rightarrow \infty. \tag{7b}$$

The dynamics in this reactive partially miscible stratification depends thus on six dimensionless parameters: the diffusivity ratios δ_B and δ_C; the Rayleigh numbers R_A, R_B, and R_C; and the ratio β of the initial concentration of B and solubility of A.

III. REACTION-DIFFUSION CONCENTRATION PROFILES

To understand the dynamics in the host phase and reconstruct the density profiles (5d) therein, we compute the RD concentration profile solutions of Eqs. (5a)–(5c) with the initial (6) and boundary (7) conditions specific to the partially miscible case and compare them to their nonreactive counterpart.

A. Nonreactive case ($\beta = 0$)

We first recall the dynamics in the nonreactive case upon dissolution of A into the host phase [12–14]. The only species present in solution is A and its diffusive concentration profile is a solution of Fick's law $\frac{\partial A}{\partial t} = \frac{\partial^2 A}{\partial z^2}$ with initial conditions (6) and boundary conditions (7) where $B = 0$ and $C = 0$. We introduce the self-similar variable $\eta = z/(2\sqrt{t})$ and thus solve $A'' + 2\eta A' = 0$, with the notation $A' = \frac{dA}{d\eta}$ and $A'' = \frac{d^2 A}{d\eta^2}$. The solution, illustrated in Fig. 2(a), is

$$A = 1 - \mathrm{erf}(\eta), \tag{8}$$

where $\mathrm{erf}(\eta)$ is the error function. Species A dissolves from the boundary $\eta = 0$ and spreads towards the bulk of the host solution. The flux J_{nr} of A dissolving through the interface into the host phase is evaluated as $J_{\mathrm{nr}} = -\frac{\partial A}{\partial z}\big|_{z=0}$ and reads

$$J_{\mathrm{nr}} = \frac{1}{\sqrt{\pi t}}, \tag{9}$$

where nr stands for nonreactive. This flux decreases in time as diffusion smoothes the concentration gradient.

B. Reactive case ($\beta \neq 0$)

In the reactive case, all three species A, B, and C contribute to the density of the host phase. The dimensionless density (5d) therefore evolves in space and time depending on the dynamic changes of the concentration profiles A, B, and C.

1. Asymptotic solutions

An analytical solution of Eqs. (5a)–(5c) can be obtained by assuming that the reaction takes place only at a reaction front that moves on a diffusive time scale. The position of the reaction front is defined as $z_f = 2\eta_f\sqrt{t}$, where $\eta_f > 0$ is a constant [39–42]. This assumption is valid in the asymptotic regime when the reaction is limited by the diffusive transport of A and B towards each other, i.e., for sufficiently large times compared to the characteristic chemical reaction time ($t \gg 1$). In this limit, species A and B are immediately and entirely consumed at the reaction front. Outside the reaction front, no reaction takes place and the concentration fields j are solutions of the diffusive equations $\delta_j j'' + 2\eta j' = 0$ with the boundary conditions

$$A = 1, \quad B' = 0, \quad C' = 0 \quad \text{for } \eta = 0, \tag{10a}$$

$$A = 0, \quad B = 0, \quad C = \gamma \quad \text{for } \eta = \eta_f, \tag{10b}$$

$$A \rightarrow 0, \quad B \rightarrow \beta, \quad C \rightarrow 0 \quad \text{for } \eta \rightarrow \infty, \tag{10c}$$

where γ is the concentration of C at the reaction front, computed with Eq. (13b). The asymptotic concentration fields in the region above the reaction front $0 \leqslant \eta \leqslant \eta_f$ denoted by U (for upper) are

$$A_U = 1 - \frac{\mathrm{erf}(\eta)}{\mathrm{erf}(\eta_f)}, \tag{11a}$$

$$B_U = 0, \tag{11b}$$

$$C_U = \gamma. \tag{11c}$$

The asymptotic concentration fields in the region below the reaction front $\eta \geqslant \eta_f$ denoted by L (for lower) are

$$A_L = 0, \tag{12a}$$

$$B_L = \beta\left(1 - \frac{\mathrm{erfc}(\eta/\sqrt{\delta_B})}{\mathrm{erfc}(\eta_f/\sqrt{\delta_B})}\right), \tag{12b}$$

$$C_L = \gamma \frac{\mathrm{erfc}(\eta/\sqrt{\delta_C})}{\mathrm{erfc}(\eta_f/\sqrt{\delta_C})}, \tag{12c}$$

where $\mathrm{erfc}(\eta) = 1 - \mathrm{erf}(\eta)$ is the complementary error function.

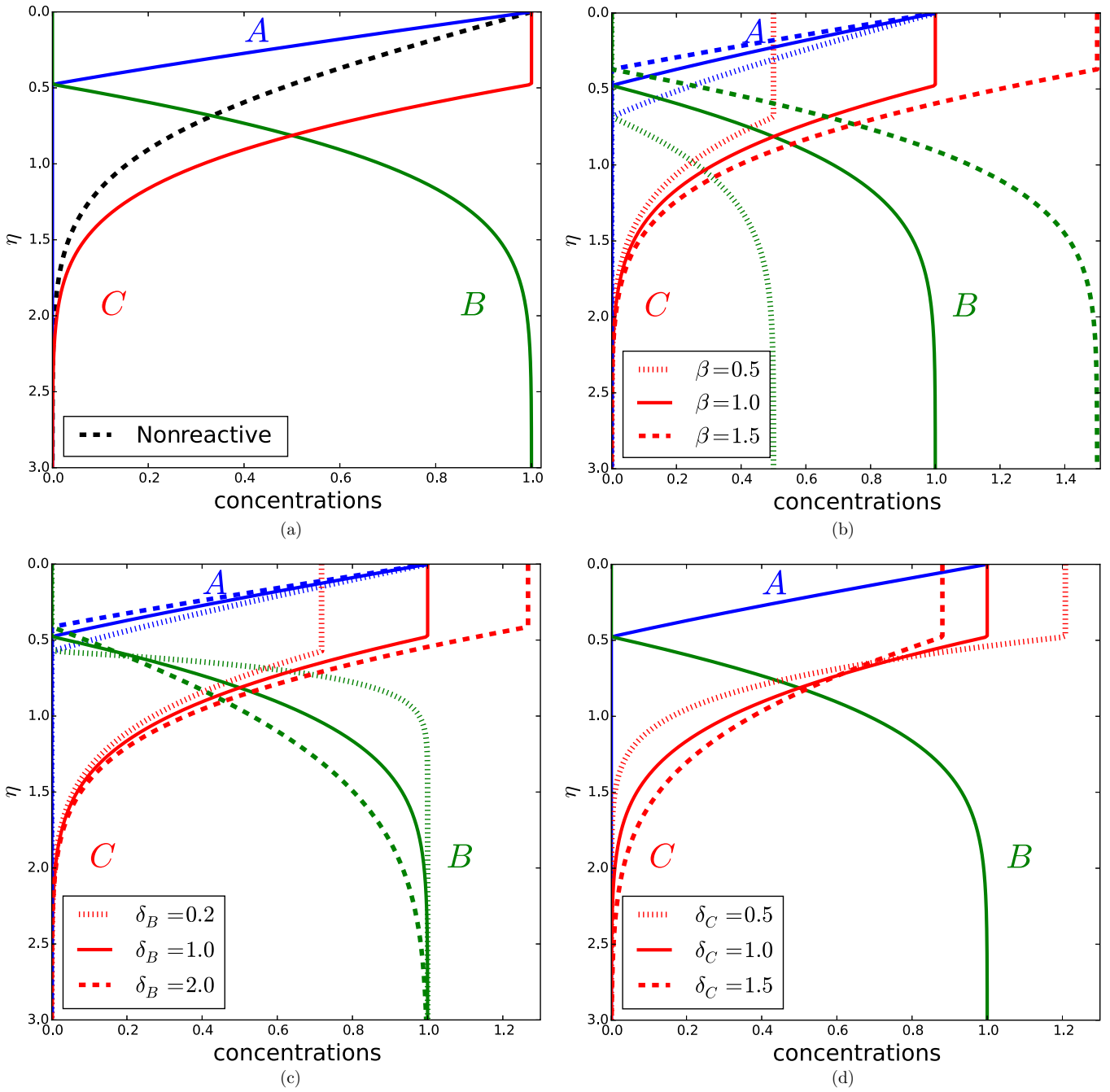

FIG. 2. Asymptotic concentration profiles (11) and (12) of A–C for (a) $\delta_B = \delta_C = \beta = 1$ compared to the nonreactive profile (8) of A (dashed black), (b) $\delta_B = \delta_C = 1$ and different β, (c) $\delta_C = \beta = 1$, and different δ_B, and (d) $\delta_B = \beta = 1$, and different δ_C.

2. *Concentration profiles*

Let us analyze the shape of the concentration profiles (11) and (12), shown in Fig. 2 for different values of parameters β, δ_B, and δ_C. Here A_U is like an error function, decreasing monotonically from the interface like the nonreactive concentration profile (8). The consumption of A by the reaction is reflected by the denominator $\mathrm{erf}(\eta_f) \leqslant 1$ in Eq. (11a): At the same coordinate η, A_U is smaller than its nonreactive counterpart [Fig. 2(a)]. This difference grows when β or δ_B increases [Figs. 2(b) and 2(c)], due to a larger flux of reactant B towards the reaction front.

Below the reaction front, B_L given by (12b) increases from 0 at the front towards its initial value β in the bulk of the solution [Fig. 2(b)]. This profile becomes sharper when δ_B decreases [Fig. 2(c)] as then weaker diffusion of B acts less efficiently at smoothing the concentration gradient. Neither A nor B depends on δ_C [Fig. 2(d)]. The concentration profiles A and B are monotonic, like their counterparts in miscible systems.

The product C accumulates in the zone $0 \leqslant \eta \leqslant \eta_f$ between the interface and the reaction front and its concentration decreases monotonically beyond $\eta > \eta_f$. The amount of

C produced increases with β and δ_B following a larger consumption of A [Figs. 2(b) and 2(c)]. Increasing δ_C does not affect the total amount of C produced, but smoothes its concentration profile because of faster diffusion [Fig. 2(d)].

3. *Position of the reaction front and maximum concentration of C*

We now examine η_f, the position of the reaction front in self-similar coordinates, and γ, the dimensionless concentration of product C at η_f. To compute η_f and γ, we invoke the fact that the reaction is diffusion limited. According to the stoichiometry of the reaction, the fluxes must be equal at the reaction front, i.e., $A'_U|_{\eta_f} = -\delta_B B'_L|_{\eta_f} = \delta_C C'_L|_{\eta_f}$, which after rearrangement gives

$$\operatorname{erfc}(\eta_f/\sqrt{\delta_B}) = \beta\sqrt{\delta_B}\operatorname{erf}(\eta_f)\exp\left[-\eta_f^2\left(\frac{1}{\delta_B}-1\right)\right], \quad (13a)$$

$$\gamma = \frac{\operatorname{erfc}(\eta_f/\sqrt{\delta_C})}{\sqrt{\delta_C}\operatorname{erf}(\eta_f)}\exp\left[\eta_f^2\left(\frac{1}{\delta_C}-1\right)\right]. \quad (13b)$$

We use a Newton-Raphson iterative method [43] to obtain η_f as a function of δ_B and β from the implicit Eq. (13a). Once η_f is known, γ can be explicitly computed as a function of δ_C and η_f using Eq. (13b).

Let us analyze how η_f and γ depend on the parameters β, δ_B, and δ_C. In the case of contact between miscible solutions of A and B, η_f can be of either sign, i.e., the reaction front can move in either direction with regard to its initial position or stay immobile, depending on the diffusivity and initial concentration ratios [31,32,39–42]. Here A progressively invades the host solution from the interface where it dissolves. Therefore, the reaction front always moves in the same direction towards positive η ($\eta_f > 0$).

The value of η_f depends on β and δ_B and determines the rate at which the front moves forward. When $\delta_B = 1$, the dependence of η_f on β is given by $\operatorname{erf}(\eta_f) = \frac{1}{\beta+1}$ [16]. More generally, η_f decreases, i.e., the motion of the reaction front slows down, when β or δ_B increases [Figs. 2(b), 2(c), and 3]. Note that for small η_f and short time, the reaction front can be assumed to be at the interface, so only the lower concentration profiles are considered [44,45]. Increasing β or δ_B amplifies the flux of fresh reactant B towards the reaction zone. This enhances the consumption of the dissolving species A, slowing down its invasion of the host phase and increasing the amount of C produced [Figs. 2(b), 2(c), and 4(a)]. Thus γ increases when β and δ_B increase. In particular, when $\delta_B = \delta_C$, γ is equal to β [15,16]. In addition, γ decreases when δ_C increases [Figs. 2(d) and 4(b)] because then the product diffuses faster away from its production zone.

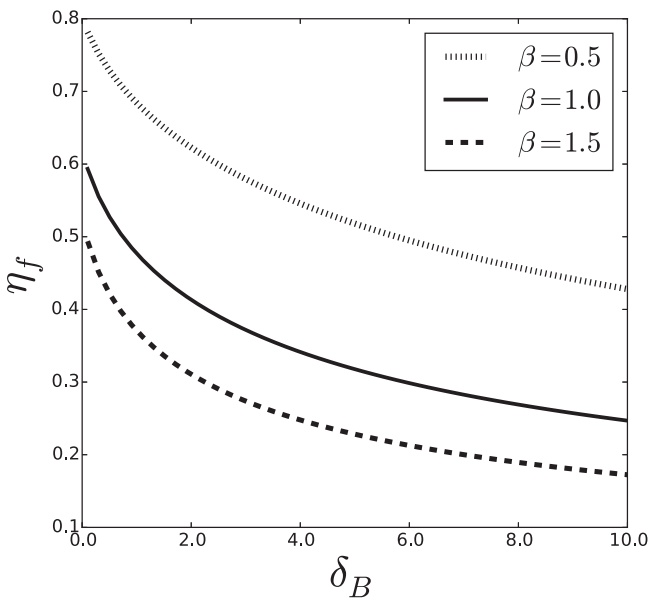

FIG. 3. Position η_f of the reaction front with regard to the interface at $\eta_f = 0$, computed with Eq. (13a), decreases when δ_B or β increases.

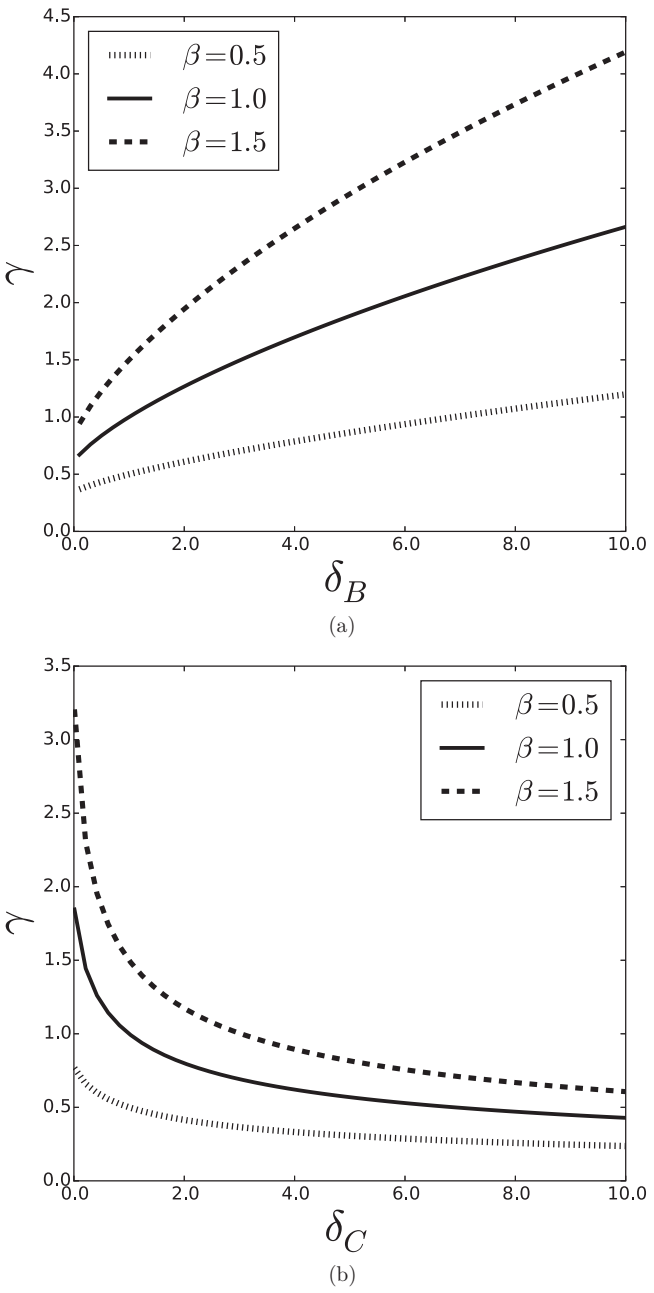

FIG. 4. Maximum product concentration γ given by (13b) is amplified when β increases or (a) δ_B increases ($\delta_C = 1$) or (b) δ_C decreases ($\delta_B = 1$).

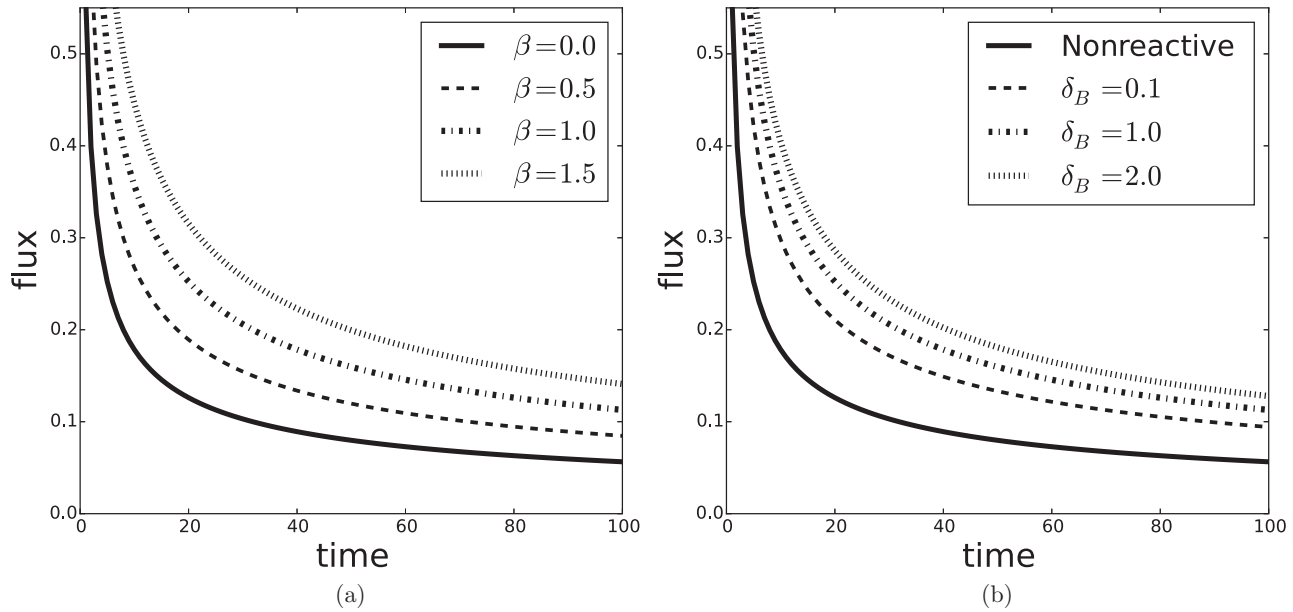

FIG. 5. The flux J [Eq. (14)] of A through the interface decreases with time and at a given time increases with (a) β ($\delta_B = 1$) and (b) δ_B ($\beta = 1$). The solid curve represents the flux $J_{\rm nr}$ in the nonreactive case Eq. (9).

4. *Flux of A through the interface*

The reactive flux $J = -\frac{\partial A_U}{\partial z}\big|_{z=0}$ of A through the interface is evaluated as

$$J = \frac{1}{\mathrm{erf}(\eta_f)\sqrt{\pi t}} = \frac{J_{\rm nr}}{\mathrm{erf}(\eta_f)}, \tag{14}$$

which shows that the flux decreases with time. As $\mathrm{erf}(\eta_f) \leqslant 1$, the reactive flux is always larger than its nonreactive counterpart (9). The difference between the reactive and nonreactive cases increases with β and δ_B, as shown in Fig. 5. When the host solution is more concentrated in B or when this species diffuses faster, the consumption of A by the reaction is indeed amplified, which accelerates the transfer of A towards the host solution.

IV. CLASSIFICATION OF THE REACTION-DIFFUSION DENSITY PROFILES

As the presence of extrema in the density profile ρ is known to affect the convective stability of the system [15,16,31,32], we search for the region in the parameter space where ρ is nonmonotonic, i.e., for which its derivative ρ' changes sign at a given location η_m.

A. Nonreactive case ($\beta = 0$)

We first consider the density profile in the nonreactive case, where ρ depends only on the concentration profile (8) of species A as [15,16]

$$\rho = R_A A = R_A[1 - \mathrm{erf}(\eta)]. \tag{15}$$

The derivative ρ' is given by

$$\rho' = R_A A' = -\frac{2}{\sqrt{\pi}} R_A e^{-\eta^2}. \tag{16}$$

The sign of ρ', depending on R_A only, is constant. Thus ρ monotonically increases along z when $R_A > 0$, decreases along z when $R_A < 0$, and is constant when $R_A = 0$.

B. Reactive case ($\beta \neq 0$)

The asymptotic RD density profiles computed by inserting solutions (11) and (12) into Eq. (5d) are

$$\rho_U = R_A\left(1 - \frac{\mathrm{erf}(\eta)}{\mathrm{erf}(\eta_f)}\right) + R_C\gamma, \tag{17a}$$

$$\rho_L = R_B\beta\left(1 - \frac{\mathrm{erfc}(\eta/\sqrt{\delta_B})}{\mathrm{erfc}(\eta_f/\sqrt{\delta_B})}\right) + R_C\gamma\,\frac{\mathrm{erfc}(\eta/\sqrt{\delta_C})}{\mathrm{erfc}(\eta_f/\sqrt{\delta_C})}. \tag{17b}$$

Equations (17) show that in the bulk solution ($\eta \to \infty$), where B is the only species contributing to the density, ρ tends to its initial value $R_B\beta$. At the reaction front η_f, where A and B are entirely consumed by the reaction and C is the only species present at concentration γ, the density is given by $\rho = R_C\gamma$. At the interface, $A = 1$, $B = 0$, $C = \gamma$ and the density is equal to $R_A + R_C\gamma$.

We now analyze the density profiles above and below the reaction front separately.

1. *Above the reaction front* ($0 \leqslant \eta \leqslant \eta_f$)

Above the reaction front, the reactant B is not present because it has been consumed by the reaction. Only A and C contribute to the density profile. The derivative ρ'_U is written as

$$\rho'_U = R_A A'_U = -\frac{2}{\sqrt{\pi}}\frac{R_A}{\mathrm{erf}(\eta_f)} e^{-\eta^2}. \tag{18}$$

Similarly to its nonreactive counterpart (see Sec. IV A), ρ_U is a monotonic function with two possibilities. If A decreases or does not change the density of the solution ($R_A \leqslant 0$),

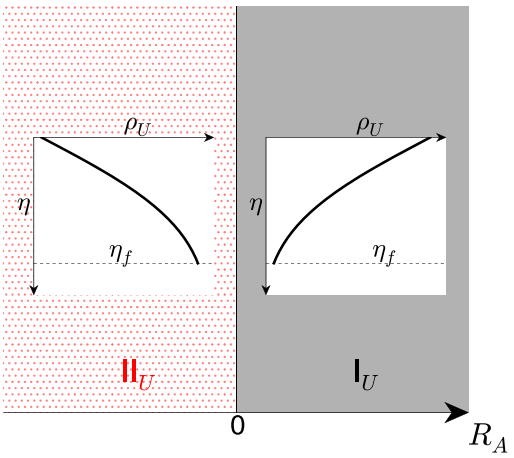

FIG. 6. Classification of the density profiles ρ_U above the reaction front ($0 \leqslant \eta \leqslant \eta_f$): monotonic increasing in zone II_U (dot hatched), constant on the boundary $R_A = 0$, and monotonic decreasing in zone I_U (shaded). The dashed line in the plots $\rho_U(\eta)$ indicates the position η_f of the reaction front.

ρ increases or remains constant from the interface towards the reaction front ($\rho_U' \geqslant 0$, zone II_U in Fig. 6). In the other case ($R_A > 0$), the density decreases from the interface towards the reaction front ($\rho_U' < 0$, zone I_U in Fig. 6). Note that in this study, the notation II will always correspond to monotonically increasing profiles and I to monotonically decreasing profiles along z. This classification does not depend on the magnitude of R_A, but only on its sign.

2. *Below the reaction front ($\eta \geqslant \eta_f$)*

Below the reaction front, two species contribute to the density profile, the dissolved reactant B and the product C, so ρ_L' reads

$$\rho_L' = R_B B_L' + R_C C_L' = \frac{2}{\sqrt{\pi}}\left(R_B \frac{\beta e^{-\eta^2/\delta_B}}{\mathrm{erfc}(\eta_f/\sqrt{\delta_B})\sqrt{\delta_B}} - R_C \frac{\gamma e^{-\eta^2/\delta_C}}{\mathrm{erfc}(\eta_f/\sqrt{\delta_C})\sqrt{\delta_C}}\right). \quad (19)$$

Therefore, the balance between both contributions $R_B B_L'$ and $R_C C_L'$ to the slope of the density profile determines whether ρ_L has an extremum or not.

Let us first mention a few trivial cases before moving to the more complex case where both species B and C increase the density of the solution. When C does not contribute to the density of the solution [$R_C = 0$, Fig. 7(a)], the density profile trivially follows the B profile and $\rho_L' = R_B B_L'$. As B increases from zero at the reaction front to its bulk value β ($B_L' > 0$, Fig. 2), ρ_L increases along z when B increases the density of the solution ($R_B > 0$, zone II_L). Conversely, when B decreases the density ($R_B < 0$, zone I_L), ρ_L decreases along z ($\rho_L' < 0$). When neither B nor C contributes to the density [boundary $R_B = 0$ in Fig. 7(a)], ρ_L is a constant ($\rho_L' = 0$). Similarly, when $R_B = 0$ but $R_C \neq 0$, the density profile follows the C profile, with C decreasing from γ at the reaction front to zero in the bulk ($C_L' < 0$, Fig. 2). Thus ρ_L decreases towards the bulk when C increases the density of the solution [$R_C > 0$, in zone I_L of Fig. 7(b)] and vice versa (not shown here).

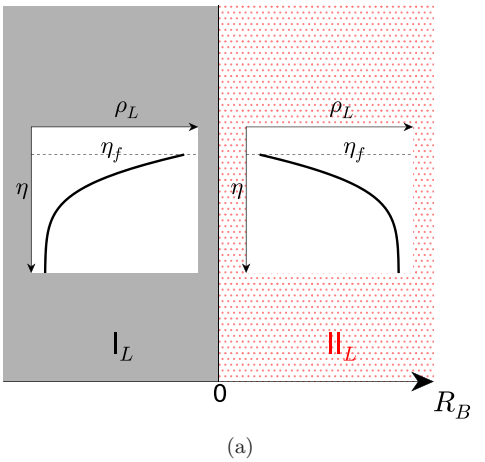

(a)

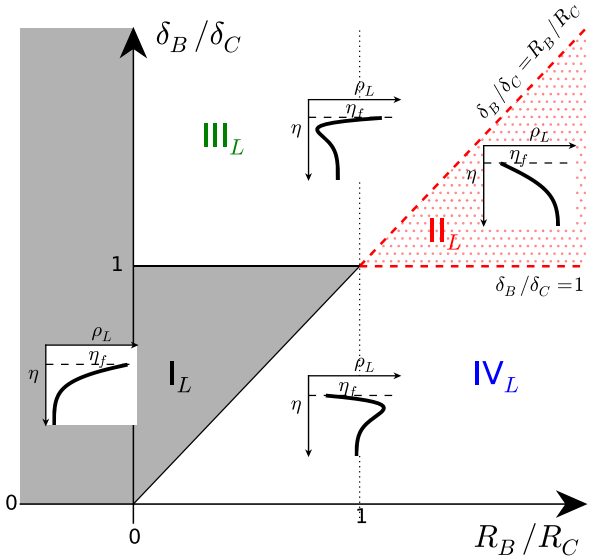

(b)

FIG. 7. Classification of the density profiles ρ_L below the reaction front ($\eta \geqslant \eta_f$) for (a) $R_C = 0$ and (b) $R_C > 0$: monotonic decreasing in zone I_L (shaded), monotonic increasing in zone II_L (dot hatched), with a minimum in zone III_L, with a maximum in zone IV_L, and constant for $R_B = R_C = 0$ or $R_B/R_C = \delta_B/\delta_C = 1$. The dashed line in the plots $\rho_L(\eta)$ indicates the position η_f of the reaction front.

Finally, the trivial case when R_B and R_C are of opposite sign can be understood as follows. As $B_L' > 0$ and $C_L' < 0$, the density gradients $R_B B_L'$ and $R_C C_L'$ are then of the same sign and the density profile is monotonic [Eq. (19)]. More specifically, the density profile decreases along z when C increases the density and B decreases it [$R_C > 0$ and $R_B < 0$, in zone I_L of Fig. 7(b)] and vice versa (not shown here).

Let us now restrict our analysis to cases where B and C increase the density of the solution (R_B and R_C positive) without loss of generality. The sign of ρ_L' can straightforwardly be deduced when R_B and R_C are negative with the relation $\rho_L'(-R_B, -R_C) = -\rho_L'(R_B, R_C)$ derived from Eq. (19).

The case $\delta_B = \delta_C$ has already been analyzed [15,16]. The density ρ_L decreases if $R_B < R_C$, is constant if $R_B = R_C$, and

otherwise increases. We now consider the most general case where B and C diffuse at different rates ($\delta_B \neq \delta_C$).

With the conditions $R_B, R_C > 0$ and $\delta_B \neq \delta_C$, we insert Eqs. (13a) and (13b) into Eq. (19) and rewrite it as

$$\rho_L' = \frac{2}{\sqrt{\pi}} \frac{e^{-\eta_f^2}}{\mathrm{erf}(\eta_f)} \frac{R_C}{\delta_B} \times \left(\frac{R_B}{R_C} e^{-(\eta^2-\eta_f^2)/\delta_B} - \frac{\delta_B}{\delta_C} e^{-(\eta^2-\eta_f^2)/\delta_C} \right). \quad (20)$$

Thus ρ_L admits an extremum at $\eta = \eta_m$ if the equality

$$\rho_L'|_{\eta_m} = 0 \Leftrightarrow \eta_m^2 - \eta_f^2 = \frac{\ln\left(\frac{R_B \delta_C}{R_C \delta_B}\right)}{\frac{1}{\delta_B} - \frac{1}{\delta_C}} \quad (21)$$

is satisfied, which is equivalent to

$$\left(\frac{\delta_B}{\delta_C} - \frac{R_B}{R_C} \right) \left(\frac{\delta_B}{\delta_C} - 1 \right) > 0, \quad (22)$$

and if

$$\rho_L''|_{\eta_m} = \frac{4\eta_m e^{-\eta_f^2}}{\sqrt{\pi}\mathrm{erf}(\eta_f)} \left(\frac{R_B \delta_C}{R_C \delta_B} \right)^{(\delta_B/\delta_C)/((\delta_B/\delta_C)-1)} \times \left(\frac{R_C}{\delta_B \delta_C} \right) \left(\frac{\delta_B}{\delta_C} - 1 \right) \neq 0. \quad (23)$$

As a consequence, ρ_L has a minimum ($\rho_L'|_{\eta_m} = 0$ and $\rho_L''|_{\eta_m} > 0$) if $\delta_B/\delta_C > \max(1, R_B/R_C)$ [zone III_L in Figs. 7(b) and 8(a)] and a maximum if $\delta_B/\delta_C < \min(1, R_B/R_C)$ [zone IV_L in Figs. 7(b) and 8(a)].

Therefore, when (22) or (23) is not satisfied, ρ_L is monotonic. As the sign of its derivative ρ_L' does not change, we determine whether ρ_L increases or decreases by looking at the sign of ρ_L' close to the reaction front,

$$\rho_L'|_{\eta \to \eta_f} \to \frac{2}{\sqrt{\pi}} \frac{e^{-\eta_f^2}}{\mathrm{erf}(\eta_f)} \frac{R_C}{\delta_B} \left(\frac{R_B}{R_C} - \frac{\delta_B}{\delta_C} \right), \quad (24)$$

and when (24) is equal to zero (i.e., when $\delta_B/\delta_C = R_B/R_C$), at the sign of $\rho_L''|_{\eta \to \eta_f}$,

$$\rho_L''|_{\eta \to \eta_f, \delta_B/\delta_C = R_B/R_C} \to \frac{4\eta_f e^{-\eta_f^2}}{\sqrt{\pi}\mathrm{erf}(\eta_f)} \frac{R_C}{\delta_C \delta_B} \left(\frac{\delta_B}{\delta_C} - 1 \right). \quad (25)$$

From the possible signs of (24) and (25), we deduce that ρ_L is monotonically decreasing if $0 < R_B/R_C \leqslant \delta_B/\delta_C < 1$ [in zone I_L of Fig. 7(b)] and monotonically increasing if $1 < \delta_B/\delta_C \leqslant R_B/R_C$ [zone II_L of Fig. 7(b)]. In conclusion, Fig. 7 summarizes the classification of the four possible lower density profiles ρ_L in the reactive system: monotonically decreasing (zone I_L), monotonically increasing (zone II_L), with a minimum (zone III_L), or with a maximum (zone IV_L), corresponding to

$$\frac{R_B}{R_C} \leqslant \frac{\delta_B}{\delta_C} \leqslant 1 \quad \text{for } R_C > 0,$$
$$R_B < 0 \quad \text{for } R_C = 0 \quad (\text{zone } \mathrm{I}_L); \quad (26a)$$
$$1 \leqslant \frac{\delta_B}{\delta_C} \leqslant \frac{R_B}{R_C} \quad \text{for } R_C > 0,$$
$$R_B > 0 \quad \text{for } R_C = 0 \quad (\text{zone } \mathrm{II}_L); \quad (26b)$$

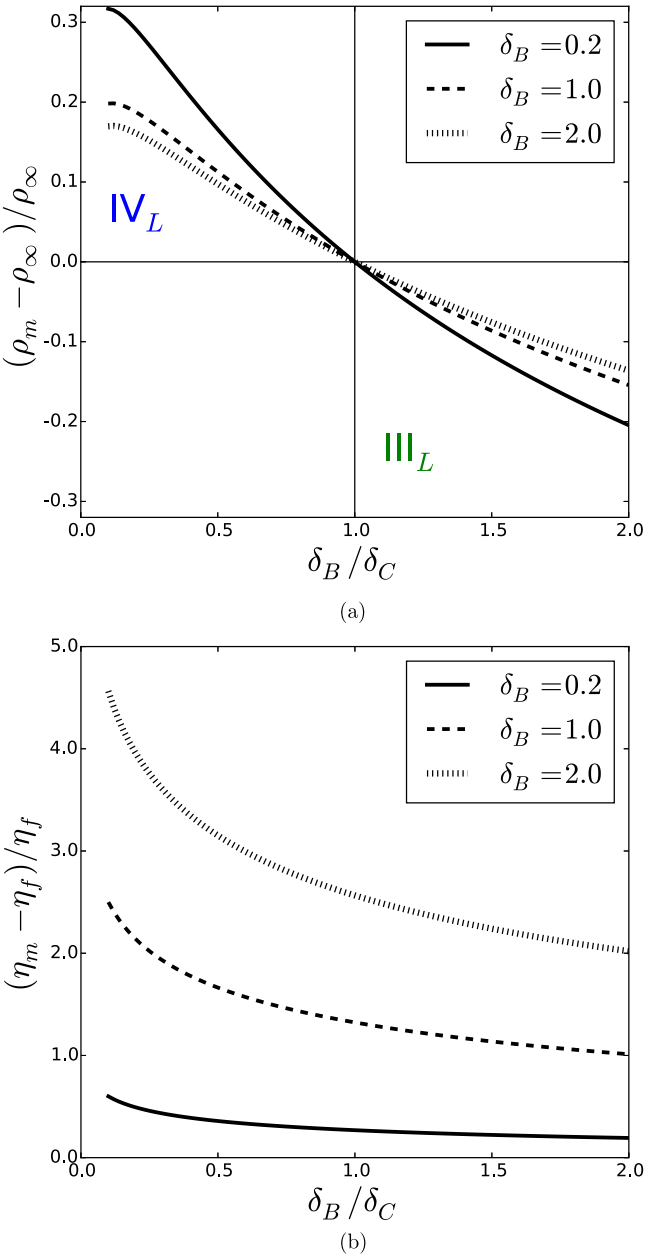

FIG. 8. Characteristics of the extremum ρ_m of density for $R_B = R_C = 1$. (a) For any value of δ_B, the relative density extremum $(\rho_m - \rho_\infty)/\rho_\infty$ becomes negative when $\delta_B/\delta_C > 1$, illustrating the transition from zone IV_L to zone III_L. (b) The relative distance $(\eta_m - \eta_f)/\eta_f$ between the extremum and the reaction front increases when δ_B/δ_C decreases or δ_B increases.

$$\frac{\delta_B}{\delta_C} > \max\left(1, \frac{R_B}{R_C}\right) \quad \text{for } R_C > 0 \quad (\text{zone } \mathrm{III}_L); \quad (26c)$$
$$\frac{\delta_B}{\delta_C} < \min\left(1, \frac{R_B}{R_C}\right) \quad \text{for } R_C > 0 \quad (\text{zone } \mathrm{IV}_L). \quad (26d)$$

V. EXTREMA BELOW THE REACTION FRONT

In zones III_L and IV_L of Fig. 7(b), the density profiles ρ_L below the reaction front have extrema because of differential diffusivity ($\delta_B \neq \delta_C$). We now analyze these extrema in detail

and in particular how their characteristics depend on the diffusivity ratio.

Figure 8(a) illustrates the transition from zone IV_L to zone III_L of Fig. 7(b) when δ_B/δ_C is increased along the line $R_B/R_C = 1$, i.e., if B and C contribute equally to the density of the solution and only differential diffusivity effects are at play. This allows one to understand the switch from a maximum to a minimum in the density profile when δ_B/δ_C is increased. The relative value of the extremum is defined as $(\rho_m - \rho_\infty)/\rho_\infty$, where $\rho_m = \rho(\eta_m)$ is the extremum of density and $\rho_\infty = \rho(\eta \rightarrow \infty) = R_B\beta$ is the density in the bulk solution. This relative value is positive in zone IV_L, as the maximum ρ_m is larger than ρ_∞, and conversely negative in zone III_L, where ρ_m is a minimum. The transition between these two zones occurs when B and C diffuse at the same rate ($\delta_B = \delta_C$). The density profile is then constant and equal to $\rho_\infty = R_B\beta$ everywhere.

The maximum of density in zone IV_L can be understood as follows. When the reactant B diffuses more slowly than the product C ($\delta_B < \delta_C$), its concentration just below the reaction front becomes larger than in the case of equal diffusivities [see Fig. 2(c)]. This can induce a maximum of density if B is sufficiently denser than C ($R_B > R_C\delta_B/\delta_C$). If this is not the case ($R_B \leqslant R_C\delta_B/\delta_C$), the density decreases monotonically (zone II_L).

Similarly, the minimum of density in zone III_L can be explained by the slower diffusion ($\delta_C < \delta_B$) and sufficiently large contribution to density of C ($R_C > R_B\delta_C/\delta_B$). The faster escape of B towards the reaction front is not compensated by the diffusion of C, as C lags behind in the upper part of the solution [see Fig. 2(d)].

In both zones III_L and IV_L, the absolute value of the extremum increases when the differential diffusivity effect becomes more important, i.e., when $|1 - \delta_B/\delta_C|$ increases. This increase is amplified with smaller δ_B [Fig. 8(a)] and δ_C (not shown here) as the concentration profiles are then sharper. Furthermore, the relative distance between the extremum and the reaction front increases when δ_B/δ_C decreases [Fig. 8(b)] and when δ_B [Fig. 8(b)] or δ_C (not shown here) increases.

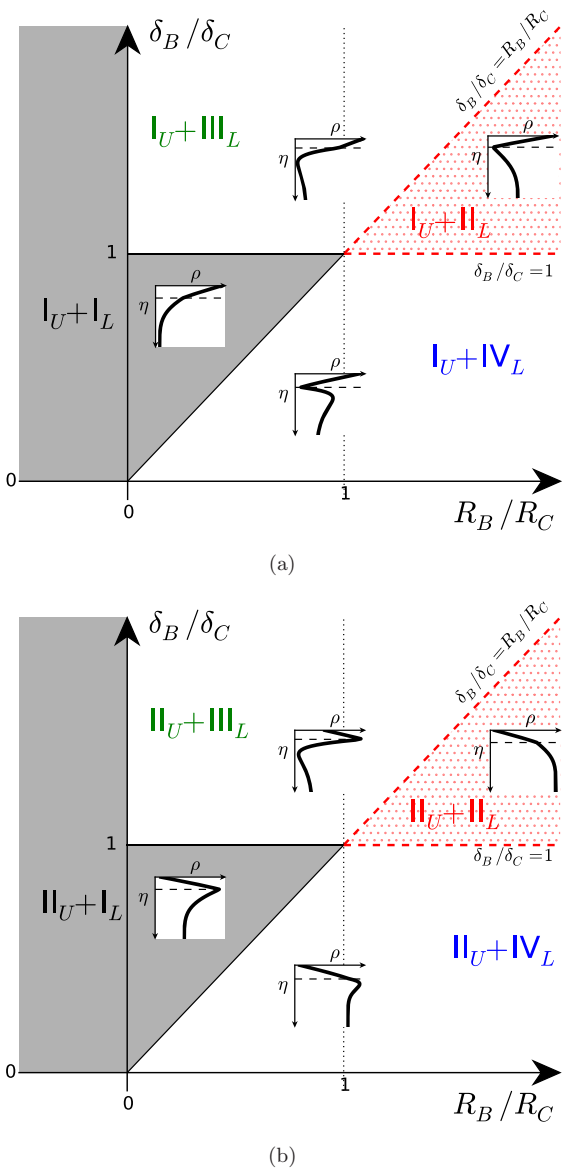

FIG. 9. Classification of the global density profiles ρ for $R_C > 0$ and (a) $R_A > 0$ or (b) $R_A < 0$. Typical plots of $\rho(\eta)$ are included, with a dashed line showing the position of the reaction front η_f.

VI. GLOBAL DENSITY PROFILES AND POSSIBLE DYNAMICS

In order to have an idea of the global density profiles in the host phase, the two types of density profiles ρ_U ($0 \leqslant \eta \leqslant \eta_f$, Fig. 6) must be combined with the four possible lower density profiles ρ_L ($\eta \geqslant \eta_f$, Fig. 7), leading to eight different possible types of density profiles: monotonic (increasing or decreasing), with one extremum (minimum or maximum, at the reaction front or below), or two extrema (minimum followed by maximum or the opposite). All these profiles are shown in Fig. 9.

Further quantitative studies such as linear stability analyses or nonlinear simulations are necessary to analyze the temporal dynamics and assess the convective stability of these density profiles for a given initial angle between the interface and gravity. The density profiles presented here are valid at large times and could thus become unstable with regard to convection before this asymptotic limit. However, their spatial dependence, i.e., the type and number of extrema, typically remains the same over time as shown previously for specific zones [15,16,46]. Therefore, we can analyze the shape of the density profiles to predict possible scenarios for the development of buoyancy-driven instabilities.

As the convective dynamics depend on the orientation of the interface with regard to gravity, we fix ideas by considering a horizontal interface. The reservoir A is on top of the denser host phase containing B and gravity points downward along z, so the initial density stratification is statically stable. We discuss which part(s) of the profile can evidently be buoyantly unstable and associate each zone with dynamics previously observed in quantitative studies (e.g., [15–17,34–38,44,45]).

A. $R_A > 0$: Chemistry can modify the characteristics of the buoyancy-driven instability

If the density of the host solution increases upon dissolution of A ($R_A > 0$), the density profile in the nonreactive case can be buoyantly unstable, as a boundary layer of denser fluid rich in A grows on top of the solution. More specifically, buoyancy-driven convection does not develop immediately, but after an onset time depending on the experimental conditions [12–14]. This is the case, e.g., of alkyl formate [17] or gaseous CO_2 [15,18,44–46] dissolving into an aqueous solution. Even when a reaction takes place in the host phase, it is not possible to observe a stratification statically stable everywhere: At least above the reaction front, the density of the solution decreases downward due to the contribution of the dissolving species to density [Fig. 9(a)].

When the upper and lower density profiles are of the same type I [zone $I_U + I_L$ in Fig. 9(a)], global density profiles are monotonically decreasing like their nonreactive counterpart (Sec. IV A). This case has been illustrated by experiments of CO_2 dissolving into a solution of monoethanolamine ($\delta_B/\delta_C \approx 1$ and $R_B/R_C \approx 0.45$) [44]. The instability develops faster than in the nonreactive case because the contribution of the product C to density adds to that of the dissolving species [15,16].

Density profiles of other zones in Fig. 9(a) have at least one minimum, at the reaction front or below, which can lead to different dynamics. In zone $I_U + II_L$, the minimum forms at the reaction front even without differential diffusivity if the product is less dense than the initially dissolved reactant ($R_C < R_B$) [15,16]. In that case, this minimum acts as a stabilizing barrier because locally less dense fluid lies on top of denser one. The instability and thus the fingering pattern observed experimentally develop more slowly than in the nonreactive case [15–17].

By contrast, the minimum of density in zone $I_U + III_L$, below the reaction front, can build up only if the product and initially dissolved reactant diffuse at different rates. This zone has been illustrated by the experiments of CO_2 dissolving into aqueous solutions of alkali metals ($\delta_B/\delta_C \approx 2$ and $R_B/R_C \approx 0.4$). In that case, the instability develops faster than without reaction [15,46]. The concentration of C above and at the reaction front is larger than in the equal diffusivities case [Figs. 2(d) and 4], which increases the density jump at the origin of convection and thus opposes the stabilizing effect of the minimum [46].

In zone $I_U + IV_L$, the minimum of density at the reaction front is followed by a maximum where denser fluid lies on top of a less dense one. We expect that this local unstable density stratification can generate buoyancy-driven convection. This type of density profile can build up during the dissolution of CO_2 into a solution of sodium carbonate and bicarbonate ($\delta_B/\delta_C \approx 0.8$ and $R_B/R_C \approx 1.11$) [44,45].

B. $R_A \leqslant 0$: Chemistry can be at the origin of buoyancy-driven instability

When the density of the host solution decreases or remains constant upon dissolution of A ($R_A \leqslant 0$), the corresponding nonreactive case is buoyantly stable. This is usually the case when a gas, e.g., oxygen [34–38], dissolves into an aqueous solution, except when that gas is CO_2 [8]. The dissolution of CO_2 can nevertheless decrease the density of some organic solvents, for example, nitrobenzene or chlorobenzene [47]. Studying the case $R_A \leqslant 0$ is also relevant in the context of CO_2 sequestration, because the density of the brine decreases upon dissolution of CO_2 with a sufficiently large fraction of hydrogen sulfide (H_2S) impurities [48,49].

If the upper and lower density profiles are both of type II increasing [zone $II_U + II_L$ in Fig. 9(b)], they combine in a global profile statically stable as everywhere less dense fluid lies on top of a denser one. Despite this statically stable stratification, this profile can still be unstable with regard to double diffusive instabilities if species B and C diffuse at different rates ($\delta_B \neq \delta_C$) [19,30,33].

Outside this zone, reactions create a maximum in the density profile, and as discussed above, this localized unstable density stratification can be at the origin of buoyancy-driven convection. This is indeed the case in the methylene-blue-glucose system corresponding to zone $II_U + I_L$ ($R_A = R_B = 0$ and $R_C > 0$) [34–38]. Unlike zones $I_U + IV_L$ and $II_U + IV_L$, the maximum is here located exactly at the reaction front. The location of the density maximum seems to affect the development of fingering as the periodic birth of fingers described by Wylock *et al.* [44,45] has not been reported in the methylene-blue–glucose system [34–38].

To the best of our knowledge, no experiment illustrates yet the development of the fingering pattern in zones $II_U + III_L$ and $II_U + IV_L$. We expect that the dynamics in these zones will look like those in zones $I_U + III_L$ and $I_U + IV_L$, respectively, although the instability could grow more slowly due to the stable density gradient above the reaction front.

VII. COMPARISON WITH MISCIBLE STRATIFICATIONS

The density profiles classified here for partially miscible systems bear some similarities and differences with their counterparts in miscible stratifications [33]. In both cases, the theoretical framework used to compute the density profiles is similar. The same RD equations can be solved to compute the concentration fields in both systems. The main difference lies in the initial and boundary conditions with a constant concentration of A imposed at the top boundary, equal to the solubility A_0 of A in the host solution for the partially miscible stratification. By contrast, for miscible stratifications, no-flux boundary conditions are imposed at $\eta \to \pm\infty$ as the system is typically isolated while the miscible interface expands diffusively in both directions around $\eta = 0$, the initial contact line. This completely changes the picture, as discussed below.

Although the expressions for the concentration profiles below the reaction front (12) have the same form in both systems, the maximum concentration γ of the product and the coordinate η_f of the reaction front are different. Moreover, the number of possible profiles is much larger in miscible fluids, where 62 profiles can be obtained [33]. Indeed, the situation above the reaction front is more complex: Density profiles with zero, one, or two extrema can develop in miscible cases because of the combination of the two opposing concentration gradients A'_U and C'_U [33]. By contrast, here only A'_U affects the type of upper density profile. Furthermore, in miscible

stratifications the front can remain at the same location or move towards positive or negative η, amplifying the number of possibilities. On the contrary, here there is only one direction possible for the movement of the reaction front: Species A can only invade the host phase from the interface where it dissolves towards positive η.

VIII. CONCLUSION

We have computed theoretically reaction-diffusion density profiles in partially miscible stratifications where a solute A dissolves into a host phase containing a solute B and an $A + B \rightarrow C$ reaction takes place. While only two different types of density profiles can develop in the nonreactive case, eight different types of profiles can be observed in the reactive case, depending on the solutal and diffusivity ratios, each potentially associated with a different type of convective dynamics. The coupling between dissolution and diffusion on the one hand and chemistry on the other multiplies the number of possible scenarios for the development of buoyancy-driven instabilities. This enlarged complexity can be explained by the increased number of parameters as three species A, B, and C are involved in the dynamics instead of only one in the nonreactive case.

This work opens possibilities for further research. We have proposed a general framework, independent of the chosen flow equation, in order to guide future quantitative experiments, linear stability analyses, or nonlinear simulations. The present study also represents a step towards a similar classification of density profiles in immiscible stratifications where the transfer of solutes between phases can be limited by diffusion and complex dynamics can appear in both phases. Further, we note that our results can easily be extended to any property of the fluid depending linearly on the concentrations of the solutes, such as surface tension. Understanding the coupling of chemistry, differential diffusivity, and fluid flow helps clarify the development of convection, for instance, in industrial setups (chemical extraction, etc.) or geological formations (CO_2 sequestration, enhanced oil recovery, natural convection in aquifers beneath saline lakes, etc.).

ACKNOWLEDGMENTS

A.D. thanks Prodex and the FNRS-PDR program Forecast for financial support. L.R. acknowledges funding from F.R.S.-FNRS and ARC program. V.L. gratefully acknowledges funding from a F.R.S.-FNRS Research Fellowship.

[1] R. Wooding, S. W. Tyler, and I. White, Water Resour. Res. **33**, 1199 (1997).
[2] J. D. Stevens, J. M. Sharp, C. T. Simmons, and T. Fenstemaker, J. Hydrol. **375**, 394 (2009).
[3] V. Alvarado and E. Manrique, Energies **3**, 1529 (2010).
[4] L. Rongy, K. B. Haugen, and A. Firoozabadi, AIChE J. **58**, 1336 (2012).
[5] A. Firoozabadi and P. Cheng, AIChE J. **56**, 1398 (2010).
[6] H. E. Huppert and J. A. Neufeld, Annu. Rev. Fluid Mech. **46**, 255 (2014).
[7] H. Emami-Meybodi, H. Hassanzadeh, C. P. Green, and J. Ennis-King, Int. J. Greenh. Gas Control **40**, 238 (2015).
[8] J. Ennis-King and L. Paterson, SPE J. **10**, 349 (2005).
[9] P. Cheng, M. Bestehorn, and A. Firoozabadi, Water Resour. Res. **48**, W09539 (2012).
[10] M. Rasmusson, F. Fagerlund, Y. Tsang, K. Rasmusson, and A. Niemi, Adv. Water Res. **84**, 136 (2015).
[11] G. De Silva, P. Ranjith, and M. Perera, Fuel **155**, 128 (2015).
[12] A. Riaz, M. Hesse, H. A. Tchelepi, and F. M. Orr, J. Fluid Mech. **548**, 87 (2006).
[13] D. A. S. Rees, A. Selim, and J. P. Ennis-King, in *Emerging Topics in Heat and Mass Transfer in Porous Media*, edited by P. Vadász, Theory and Applications of Transport in Porous Media Vol. 22 (Springer Netherlands, New York, 2008), pp. 85–110.
[14] V. Loodts, L. Rongy, and A. De Wit, Chaos **24**, 043120 (2014).
[15] V. Loodts, C. Thomas, L. Rongy, and A. De Wit, Phys. Rev. Lett. **113**, 114501 (2014).
[16] V. Loodts, L. Rongy, and A. De Wit, Phys. Chem. Chem. Phys. **17**, 29814 (2015).
[17] M. A. Budroni, L. A. Riolfo, L. Lemaigre, F. Rossi, M. Rustici, and A. De Wit, J. Phys. Chem. Lett. **5**, 875 (2014).
[18] C. Thomas, L. Lemaigre, A. Zalts, A. D'Onofrio, and A. De Wit, Int. J. Greenh. Gas Control **42**, 525 (2015).
[19] J. S. Turner, *Buoyancy Effects in Fluids* (Cambridge University Press, Cambridge, 1979).
[20] E. Guyon, J.-P. Hulin, L. Petit, and C. Mitescu, *Physical Hydrodynamics* (Oxford University Press, Oxford, 2001).
[21] J. E. Simpson, *Gravity Currents in the Environment and the Laboratory* (Cambridge University Press, Cambridge, 1997).
[22] M. A. Hesse, F. M. Orr, and H. A. Tchelepi, J. Fluid Mech. **611**, 35 (2008).
[23] A. C. Slim and T. S. Ramakrishnan, Phys. Fluids **22**, 124103 (2010).
[24] A. C. Slim, M. M. Bandi, J. C. Miller, and L. Mahadevan, Phys. Fluids **25**, 024101 (2013).
[25] M. Lappa, C. Piccolo, and L. Carotenuto, Colloids Surf. A **261**, 177 (2005).
[26] D. Bratsun, K. Kostarev, A. Mizev, and E. Mosheva, Phys. Rev. E **92**, 011003(R) (2015).
[27] C. Almarcha, P. M. J. Trevelyan, P. Grosfils, and A. De Wit, Phys. Rev. Lett. **104**, 044501 (2010).
[28] L. Lemaigre, M. A. Budroni, L. A. Riolfo, P. Grosfils, and A. De Wit, Phys. Fluids **25**, 014103 (2013).
[29] J. Carballido-Landeira, P. M. J. Trevelyan, C. Almarcha, and A. De Wit, Phys. Fluids **25**, 024107 (2013).
[30] P. M. J. Trevelyan, C. Almarcha, and A. De Wit, J. Fluid Mech. **670**, 38 (2011).
[31] L. Rongy, P. M. J. Trevelyan, and A. De Wit, Phys. Rev. Lett. **101**, 084503 (2008).
[32] L. Rongy, P. M. J. Trevelyan, and A. De Wit, Chem. Eng. Sci. **65**, 2382 (2010).
[33] P. M. J. Trevelyan, C. Almarcha, and A. De Wit, Phys. Rev. E **91**, 023001 (2015).

[34] M. A. Bees, A. J. Pons, P. G. Sørensen, and F. Sagués, J. Chem. Phys. **114**, 1932 (2001).
[35] A. J. Pons, F. Sagués, M. A. Bees, and P. G. Sørensen, J. Phys. Chem. B **104**, 2251 (2000).
[36] A. J. Pons, F. Sagués, M. A. Bees, and P. G. Sørensen, J. Phys. Chem. B **106**, 7252 (2002).
[37] A. J. Pons, O. Batiste, and M. A. Bees, Phys. Rev. E **78**, 016316 (2008).
[38] T. Köllner, M. Rossi, F. Broer, and T. Boeck, Phys. Rev. E **90**, 053004 (2014).
[39] L. Gàlfi and Z. Ràcz, Phys. Rev. A **38**, 3151 (1988).
[40] Z. Jiang and C. Ebner, Phys. Rev. A **42**, 7483 (1990).
[41] S. Cornell, Z. Koza, and M. Droz, Phys. Rev. E **52**, 3500 (1995).
[42] Z. Koza, J. Stat. Phys. **85**, 179 (1996).
[43] J. D. Faires and R. L. Burden, *Numerical Methods*, 4th ed. (Brooks/Cole, Cengage Learning, Boston, 2013).
[44] C. Wylock, A. Rednikov, B. Haut, and P. Colinet, J. Phys. Chem. B **118**, 11323 (2014).
[45] C. Wylock, A. Rednikov, P. Colinet, and B. Haut, Chem. Eng. Sci. (2016), doi:10.1016/j.ces.2016.04.061.
[46] C. Thomas, V. Loodts, L. Rongy, and A. De Wit, Int. J. Greenh. Gas Control **53**, 230 (2016).
[47] A. Okhotsimskii and M. Hozawa, Chem. Eng. Sci. **53**, 2547 (1998).
[48] X. Ji and C. Zhu, Environ. Sci. Technol. **47**, 55 (2013).
[49] S. M. Jafari Raad and H. Hassanzadeh, Int. J. Greenh. Gas Control **54**, 250 (2016).